NAVAL POSTGRADUATE SCHOOL
Monterey, California

1450

AD-A257 553

DTIC
ELECTE
DEC 0 1 1992
S **A** **D**

THESIS

THE EFFECTS OF MIXED LAYER DYNAMICS ON ICE
GROWTH IN THE CENTRAL ARCTIC

by

Bruce R. Kitchen

September, 1992

Thesis Advisor: Roland W. Garwood

92-30418

9?

REPORT DOCUMENTATION PAGE

1a. REPORT SECURITY CLASSIFICATION UNCLASSIFIED	1b. RESTRICTIVE MARKINGS
2a. SECURITY CLASSIFICATION AUTHORITY	3. DISTRIBUTION/AVAILABILITY OF REPORT
2b. DECLASSIFICATION/DOWNGRADING SCHEDULE	Approved for public release; distribution is unlimited.

4. PERFORMING ORGANIZATION REPORT NUMBER(S)	5. MONITORING ORGANIZATION REPORT NUMBER(S)

6a. NAME OF PERFORMING ORGANIZATION Naval Postgraduate School	6b. OFFICE SYMBOL (If applicable) 35	7a. NAME OF MONITORING ORGANIZATION Naval Postgraduate School
6c. ADDRESS (City, State, and ZIP Code) Monterey, CA 93943-5000		7b. ADDRESS (City, State, and ZIP Code) Monterey, CA 93943-5000

8a. NAME OF FUNDING/SPONSORING ORGANIZATION	8b. OFFICE SYMBOL (If applicable)	9. PROCUREMENT INSTRUMENT IDENTIFICATION NUMBER
8c. ADDRESS (City, State, and ZIP Code)		10. SOURCE OF FUNDING NUMBERS

Program Element No.	Project No.	Task No.	Work Unit Accession Number

11. TITLE (Include Security Classification)
THE EFFECTS OF MIXED LAYER DYNAMICS ON ICE GROWTH IN THE CENTRAL ARCTIC

12. PERSONAL AUTHOR(S) Kitchen, Bruce R.

13a. TYPE OF REPORT Master's Thesis	13b. TIME COVERED From To	14. DATE OF REPORT (year, month, day) September 1992	15. PAGE COUNT 101

16. SUPPLEMENTARY NOTATION
The views expressed in this thesis are those of the author and do not reflect the official policy or position of the Department of Defense or the U.S. Government.

17. COSATI CODES			18. SUBJECT TERMS (continue on reverse if necessary and identify by block number)
FIELD	GROUP	SUBGROUP	Oceanography, Sea Ice, Mixed Layer Modeling

19. ABSTRACT (continue on reverse if necessary and identify by block number)

The thermodynamic model of Thorndike (1992) is coupled to a one dimensional, two layer ocean entrainment model to study the effect of mixed layer dynamics on ice growth and the variation in the ocean heat flux into the ice due to mixed layer entrainment. Model simulations show (i) the existance of a negative feedback between the ice growth and the mixed layer entrainment; (ii) the underlying ocean salinity has a greater effect on the ocean heat flux than does variations in the underlying ocean temperature. Model simulations for a variety of surface forcings and initial conditions demonstrate the need to include mixed layer dynamics for realistic ice prediction in the arctic.

20. DISTRIBUTION/AVAILABILITY OF ABSTRACT ☐ UNCLASSIFIED/UNLIMITED ☒ SAME AS REPORT ☐ DTIC USERS	21. ABSTRACT SECURITY CLASSIFICATION Unlassified	
22a. NAME OF RESPONSIBLE INDIVIDUAL Roland W. Gaarwood	22b. TELEPHONE (Include Area code) (408) 646-3260	22c. OFFICE SYMBOL OC/Gd

DD FORM 1473, 84 MAR   83 APR edition may be used until exhausted   SECURITY CLASSIFICATION OF THIS PAGE
All other editions are obsolete   Unclassified

The Effects of Mixed Layer Dynamics on Ice Growth in the Central Arctic

by

Bruce R. Kitchen
Lieutenant Commander, United States Navy
B.S., Virginia Military Institute

Submitted in partial fulfillment
of the requirements for the degree of

MASTER OF SCIENCE IN METEOROLOGY AND PHYSICAL OCEANOGRAPHY
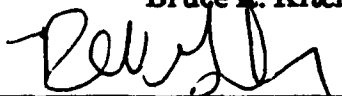
from the

NAVAL POSTGRADUATE SCHOOL
September 1992

Author: _____
Bruce R. Kitchen

Approved by: _____
Roland W. Garwood, Thesis Advisor

_____
Alan S. Thorndike, Second Reader

_____
Curtis A. Collins, Chairman
Department of Oceanography

ABSTRACT

The thermodynamic ice model of Thorndike (1992) is coupled to a one dimensional, two layer ocean entrainment model to study the effect of mixed layer dynamics on ice growth and the variation in the ocean heat flux into the ice due to mixed layer entrainment. Model simulations show (i) the existence of a negative feedback between the ice growth and the mixed layer entrainment; and (ii) the underlying ocean salinity has a greater effect on the ocean heat flux than does variations in the underlying ocean temperature. Model simulations for a variety of surface forcing and initial conditions demonstrate the need to include mixed layer dynamics for realistic ice prediction in the Arctic.

TABLE OF CONTENTS

ACKNOWLEDGEMENTS

The author would like to thank and extend my highest regard for the support, guidance and patience of Professors Roland W. Garwood and Alan S. Thorndike in the conduct of the research and preparation of this thesis. Additionally, I want to thank all the people, too numerous to name, at the Naval Postgraduate School for their assistance and support they provided throughout this research. Finally, I thank my wife, Trish for her extra patience, support and love, without which I would never have been able to complete this research.

I. INTRODUCTION

A. BACKGROUND

The thermodynamic growth of sea ice is essentially a one-dimensional heat conduction problem with the boundary conditions expressed in terms of incident heat fluxes of shortwave and longwave radiation and sensible heat at the surface and the upward, sensible heat flux from the ocean (Untersteiner, 1961). The heat budget is approximately one-dimensional because sea ice is very thin in comparison to the large area it covers, and small changes in the atmospheric or oceanic heat fluxes can cause major changes in sea ice thickness and extent (Maykut, 1985). The surface temperature of the ice will vary, according to Kirchoff's Law (Stewart, 1985), so the outgoing longwave radiation nearly balances the incoming fluxes at the surface. When the surface temperature of the ice is less than the freezing temperature of the ice a temperature gradient is set up across the ice and heat heat will be conducted upwards through the ice. If this conductive flux exceeds the oceanic heat flux due to entrainment, latent heat will be released at the bottom of the ice in the form of ice growth (Thorndike, 1992).

Early thermodynamic sea-ice models (Untersteiner, 1964; Maykut and Untersteiner, 1971; Washington et al., 1976) used observed or calculated atmospheric forcing with prescribed upward ocean heat flux into the ice. The next development was coupled ice-ocean models to include ocean dynamics. Parkinson and Washington (1979) used a mixed layer of fixed depth and a fixed value for the upward oceanic heat flux. Hibler and Bryan (1987) coupled a dynamic thermodynamic sea ice model to a multi-level baroclinic ocean model, and Semtner (1987) coupled a dynamic thermodynamic sea ice model to a multi-level primitive equation ocean circulation model. Both of these later models calculated the upward oceanic heat flux by comparing the temperature difference between the ice and the upper level of the ocean model. Although full mixed layer dynamics are not used in these models to calculate the upward oceanic heat flux, they do show the sensitivity of ice thickness and extent to the ocean heat flux. It was not until Lemke (1987) coupled a thermodynamic sea ice model with a one dimensional, ocean mixed layer model that the vertical oceanic heat flux was determined using mixed layer physics. However, his model empirically paramaterizes the mechanical mixing due to ice motion. Mellor and Kantha (1989) also developed a coupled ice-ocean mixed layer model utilizing second order closure to determine ocean eddy conductivity.

Claes (1990) showed the impact of mixed layer dynamics on the onset of freezing and determined that, under certain conditions, the upward oceanic heat flux could prevent ice formation regardless of the atmospheric forcing.

2

B. OBJECTIVE

The fluxes of momentum, mass, and heat into the ocean are controlled by the oceanic surface mixed layer so proper understanding of mixed layer dynamics is critical to understanding the physical oceanography of the arctic.

For this research a simplified, sea ice model (Thorndike, 1992) is coupled with a tunable variation of the Kraus and Turner (1967) one-dimensional mixed layer model to investigate the effect of mixed layer dynamics on the thickness of sea ice and the variation in the ocean heat flux into the ice. The tunable mixing coefficients in the mixed layer model are determined by solving the Naval Postgraduate School bulk turbulence closure model (Garwood, 1977). The simplicity of the Kraus-Turner model simplifies the investigation of the thermodynamic and dynamic interactions of the ocean mixed layer and sea ice under diverse conditions. Cases that need to be studied include ice response to storms under varying initial temperature and salinity profiles, the seasonal cycle of refreezing and melting, and longer-term climatic response to differing initial thermodynamic conditions beneath the ice.

Chapter II discusses processes involved in sea ice growth and ocean mixed layer dynamics. In Chapter III the sea ice model is developed and coupled with the ocean mixed layer model. Chapter IV will give case studies using varying initial conditions to demonstrate the sensitivity of the model to different forcing and the interaction between dynamic and thermodynamic

3

processes. Chapter V summarizes the results of the research, and makes

conclusions and recommendations for further study.

II THEORY

A. FORMATION AND GROWTH OF SEA ICE

The presence of salt in seawater depresses both the freezing temperature of the water and the temperature of maximum density, compared to fresh water. Usually, the salinity of seawater is greater than 24.7 psu, so the freezing temperature is higher than the temperature of maximum density. Hence, as the surface of the ocean cools, the surface water density increases and convective mixing results. This cooling will continue until the mixed layer is at the freezing point (Weeks and Ackley, 1982). However, the underlying thermodynamic structure of the ocean is a significant factor in determining the possible onset of freezing (Claes, 1990).

When the mixed layer temperature has reached the freezing point any additional heat loss causes the water to be supercooled, and ice begins to form. The amount of supercooling required to cause ice formation is on the order of only a few hundredths of a degree Celsius and leads to the production of Frazil ice (Maykut, 1985). Depending on wind and wave action the continued production of frazil ice results in "sheet ice," grease ice, or pancake ice (Weeks and Ackley, 1982).

Ice formation from supercooling will continue until the ice forms a continuous sheet that tends to insulate the seawater from the atmosphere. As freezing continues, the temperature of the ice surface cools from near the freezing point to a temperature that approaches the atmospheric temperature. This results in a temperature gradient across the ice and a conductive heat flux upward through the ice, removing latent heat from the ocean. Additional ice growth occurring on the underside of the sheet (Maykut, 1985) is known as congelation growth (Gow and Tucker, 1991). This new ice continues to develop and may form different types of ice depending on environmental conditions. These ice characteristics are important for understanding and predicting ice growth, and ice may be classified by stage of development as shown in Table 2.1 (Naval Polar Oceanography Center, 1984).

The amount of salt initially trapped as brine in sea ice is a function of the freezing rate of the sea water and its salinity. The makeup and distribution of salt in the ice with time will be determined by the temperature of the ice and the phase relationship between the ice, salt and brine (Gow and Tucker, 1991). Figure 2.1 shows idealized vertical salinity profiles of sea ice.

Gow and Tucker (1991) summarized the important features of the salinity profiles as follows:

- High salinities at the top and bottom of thinner ice sheets, leading to strongly C-shaped salinity profiles.
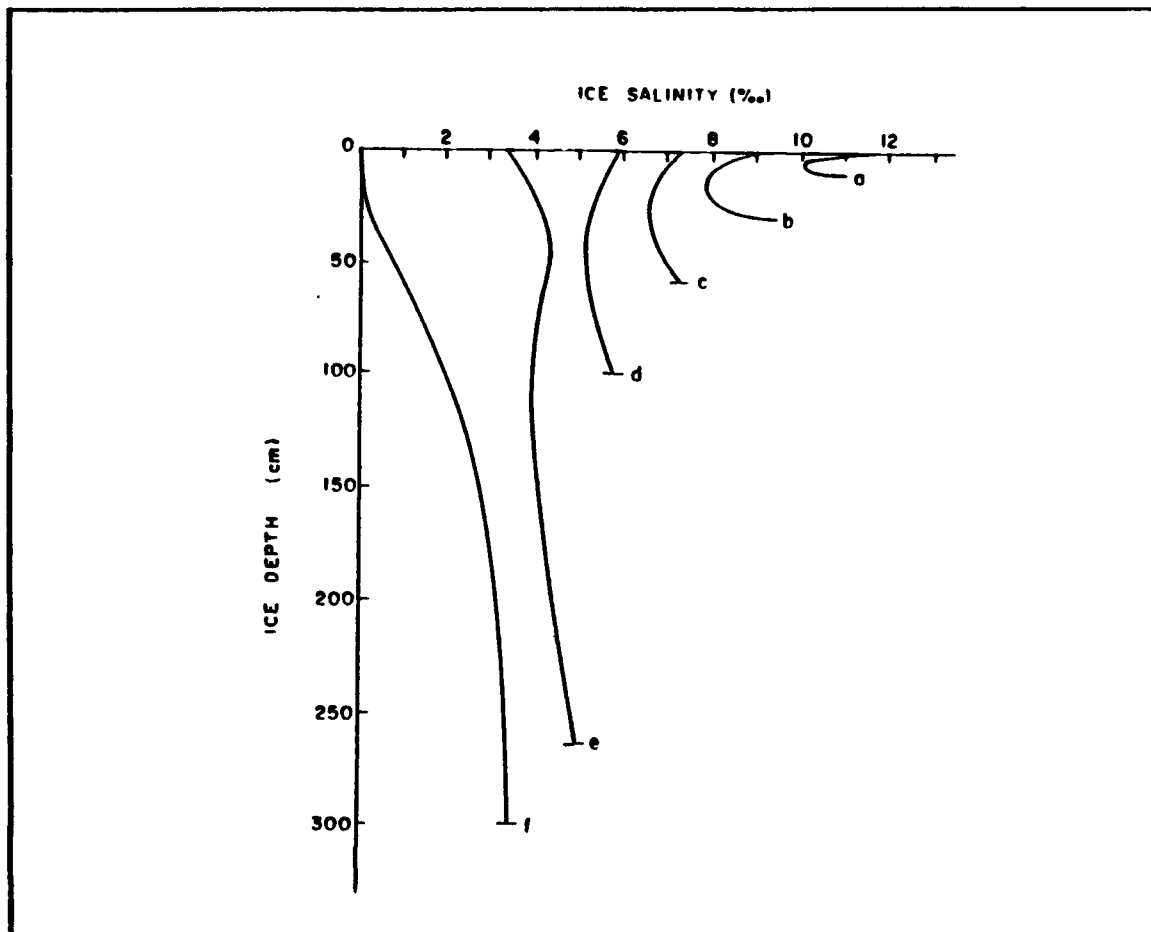
Figure 2.1 Idealized Ice Salinity Profiles in Arctic Sea Ice for Various Ice Thicknesses. Curves a - d Represent First Year Ice. The Remaining Curves Illustrate Profiles Found in Multiyear Ice (Maykut, 1985)

- General weakening of the C-shaped salinity profile accompanied by progressive decrease in bulk salinity with increasing thickness and age of the ice sheet, indicative of downward migration of brine through the ice and its ejection into the underlying ocean.

- Virtual desalinization of the upper levels of first year ice during and after its transformation to multiyear ice.

The shape of the profiles in Figure 2.1 can be explained by four

mechanisms that remove brine from sea ice: migration of brine pockets through

ice crystals, brine expulsion, brine drainage, and flushing (Untersteiner, 1968).

Brine drainage is probably the primary mechanism for the salinity changes in

first year ice (Maykut, 1985). Cox and Weeks (1974) gathered a wide variety of

data to show the dependence of average salinity upon ice thickness in the

arctic. Figure 2.2 shows that for cold (growing) ice there is a steep, linear
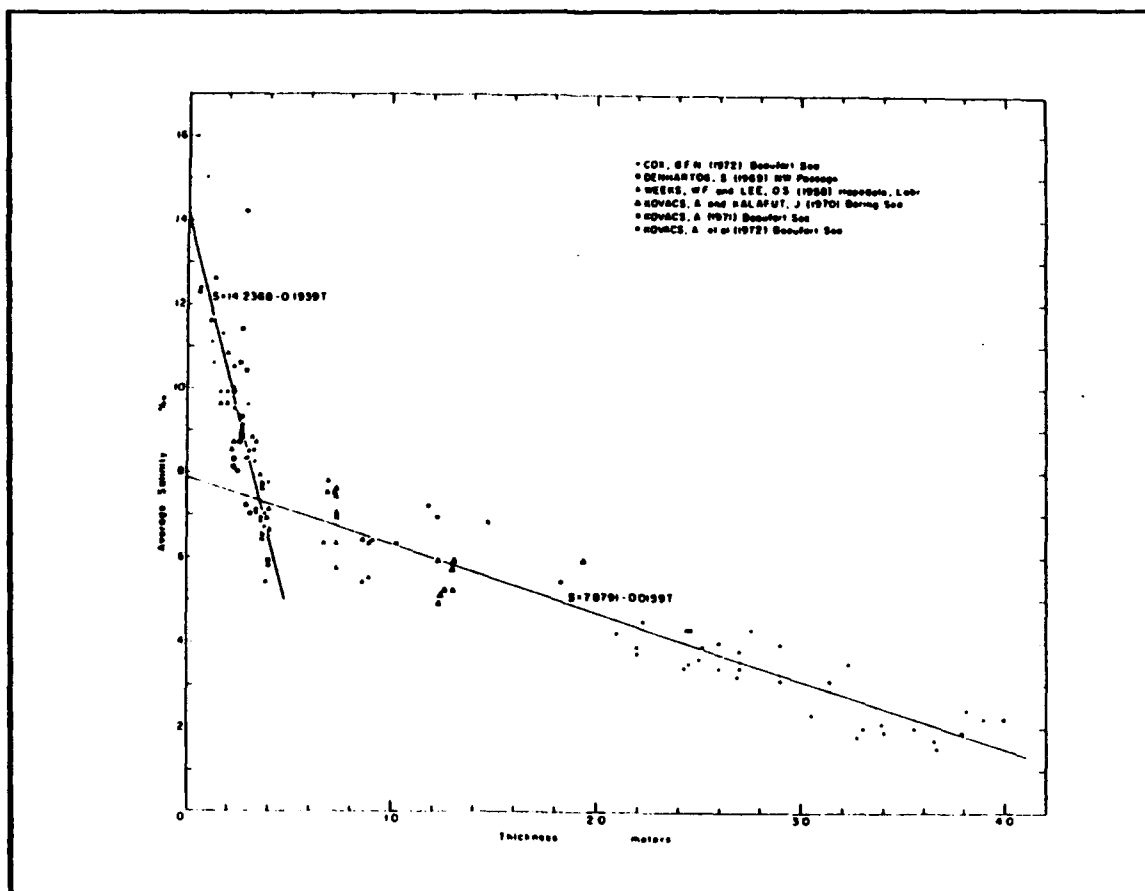
Figure 2.2 Average Salinity of Sea Ice as a Function of Ice Thickness for Cold
Sea Ice Sampled During the Growth Season (Cox and Weeks, 1974).

decrease in the average salinity of the ice up to an ice thickness of about 40

cm, and then a sharp decrease in the slope of salinity change per ice thickness

change. The abrupt change in the slope is most likely caused by a shift in the

desalinization mechanism from brine expulsion to brine drainage (Gow and

Tucker, 1991). The high initial salinity of sea ice results from the high initial

TABLE 2.1 STAGES OF ICE DEVELOPMENT

STAGE OF DEVELOPMENT	THICKNESS
New, Frazil, Slush, Shuga, Grease	0 - 10 cm (0-4 in)
Dark Nilas	0 - 5 cm (0-2 in)
Light Nilas	5 - 10 cm (2-4 in)
Gray	10 - 15 cm (4-6 in)
Gray-White	15 - 30 cm (6-12 in)
First Year Thin	30 - 70 cm (12-28 in)
First Year Medium	70 - 120 cm (28-47 in)
First Year Thick	120 -200 cm (47-80 in)
Second Year	> 2 m (> 80 in)
Multiyear	> 2 m (> 80 in)

growth rate of the ice that entraps large amounts of brine. As the ice thickens,

the growth rate of the ice slows and less brine is trapped. The effects of brine

drainage become evident and result in a decrease in the salinity of the ice

(Maykut,1985).

9

For simplicity in this research, the ice salinity will be assumed constant in time, but the Cox and Weeks data can be used to express ice salinity as a function of thickness.

B. MIXED LAYER DYNAMICS

The oceanic planetary boundary layer or mixed layer is the fully turbulent region above the seasonal thermocline. Shear stress and upward buoyancy flux provide the mechanical energy to mix salinity, momentum and heat in the mixed layer (Garwood, 1977). The shear stress is imparted by the wind to the water and transmitted downwards. The buoyancy flux results from either heating from below, cooling from above or downward surface salinity flux which leads to instabilities in the mixed layer.

The mixed layer is generally considered to be vertically homogeneous in temperature, salinity and density despite the presence of the fine scale microstructure (Zilitinkevich et al., 1979). The quasi-homogeneous nature of the mixed layer has led to it being described as a "slab." By assuming the mixed layer is homogeneous the momentum and buoyancy fluxes only need to be specified at the surface and calculated at the base of the mixed layer. However, the small variations in the mean flow, temperature or salinity can lead to large changes in the turbulent fluxes (Garwood, 1977). Zilitinkevich et al (1979) show that the vertical heat flux from a 0.01° C temperature difference in the upper 10 meters of the ocean is equivalent to the heat flux generated by a

10

1°C difference between the sea surface and the atmosphere at a height of 10 meters. Figure 2.3 shows a temperature and salinity profile taken at an AIDJEX camp (Bauer et al, 1980). The profiles clearly show the finescale structure present in the mixed layer that is not shown in the typical temperature and salinity profiles in Figure 2.4. Garwood (1977) showed that by using a vertically integrated (bulk) model of the mixed layer the important effects of the fine scale structure of the mixed layer can be accounted for by direct estimation of averaged mixed layer turbulent Kinetic energy.

The Arctic ocean mixed layer has some unique characteristics due to its ice cover. Here the shear stress between the ice and ocean provides the mechanism to transfer momentum from the atmosphere to the ocean. Typically, the ice-covered mixed layer is at or near the freezing point so it stores almost no sensible heat (McPhee, 1986). Because the density of water near the freezing point is almost entirely a function of salinity, the buoyancy flux is proportional to the salt flux alone (Morison and Smith, 1981).

The central Arctic is divided into Canadian and Eurasian basins by the Lomonosov Ridge. Coachman and Aagaard (1974) defined the three water masses in the central Arctic: Arctic water (0-200 m), Atlantic water (200-900 m) and bottom water (900 m-bottom). The Arctic water can be further divided into Arctic surface and Arctic subsurface layer waters. Figure 2.4 shows typical temperature and salinity profiles for both basins of the arctic.
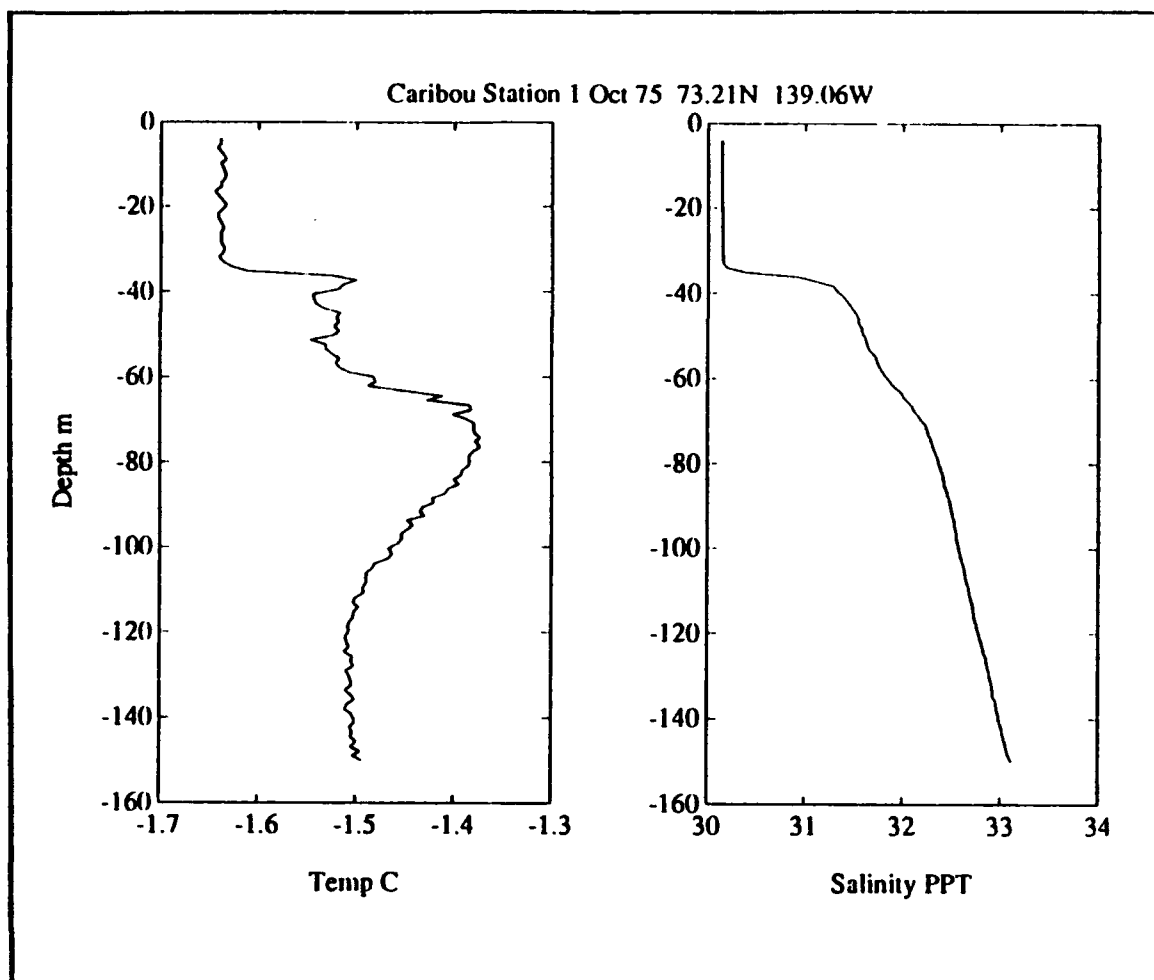
Figure 2.3 Temperature and Salinity Profiles Taken With a CTD During AIDJEX from Ice Camp Caribou Showing the Finescale Structure That is Typically Present in the Mixed Layer (Bauer et al, 1980).

The Arctic surface water extends from the surface to a 30 m-50 m depth and has fairly uniform distributions of temperature and salinity across the Arctic. The variations in salinity are mainly due to freshwater runoff from land and inflow of Atlantic and Pacific Ocean waters, but this is along the periphery of the basins. The temperature is at or near the freezing point throughout the basins except for areas that are ice-free for extended periods.
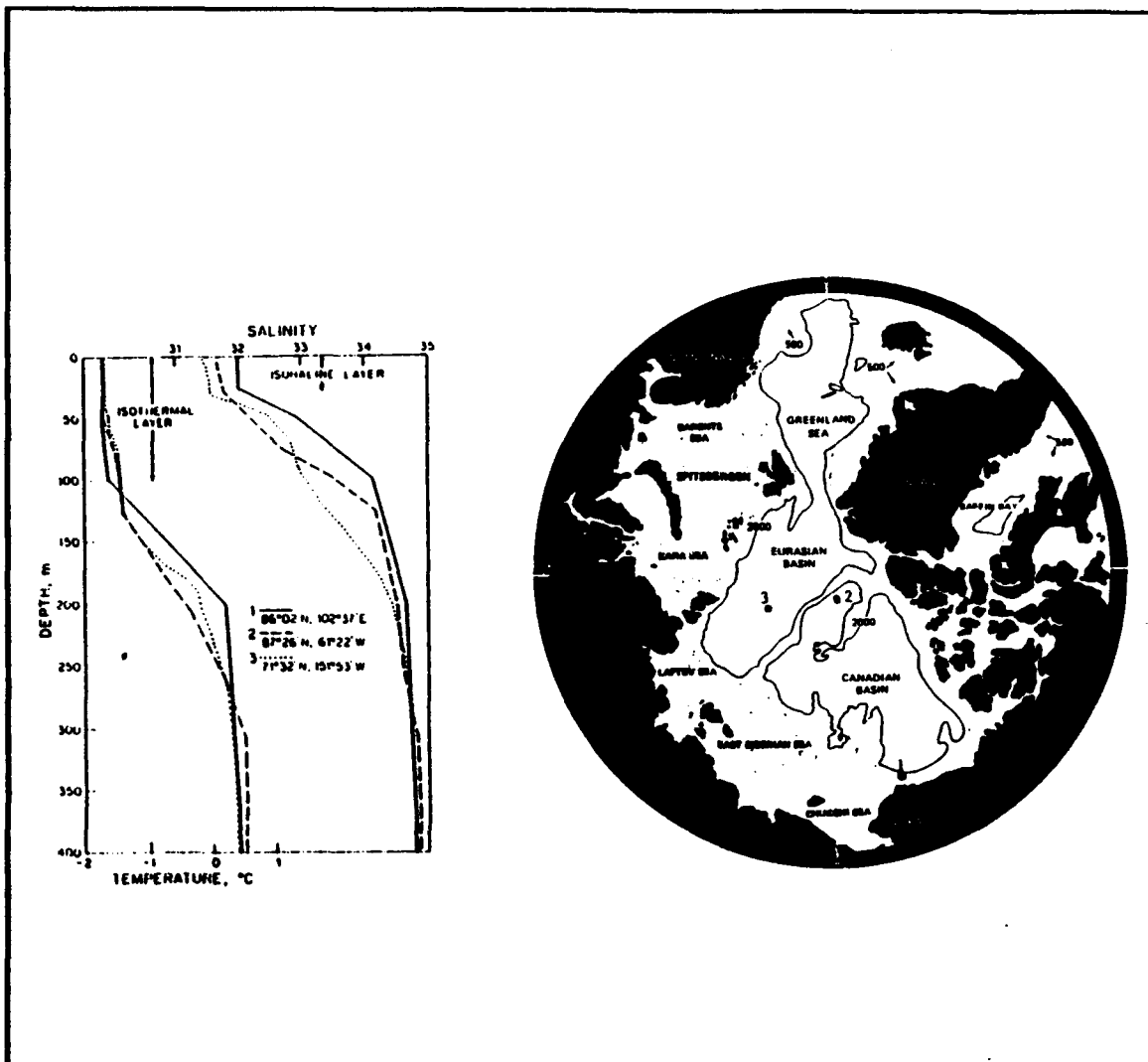
Figure 2.4 Vertical Temperature and Salinity Distribution in the upper 400 m as Observed During Winter at the Three Locations Indicated (after Coachman and Aagard, 1974).

The characteristics of the Arctic subsurface layers extend from the surface waters to 200 m and vary between the two basins. In the Eurasian basin the salinity increases with depth down to about 200 m where it reaches a value of 34.9 to 35.0 psu, and below there it is nearly isohaline. The temperature remains isothermal

13

down to about 100 m and then increases to above 0° C due to the presence of the Atlantic water. In the Canadian basin, the halocline is similar to the Eurasian basins except there is not as rapid an increase in salinity with depth. The major Canadian basin difference is in the temperature profile due to the presence of Bering sea water, which results in a temperature maximum of approximately -1° C at 75 to 100 m depth. The temperature then decreases to -1.5° C at about 150 m and remains nearly isothermal down to the Atlantic water. The presence of the Bering sea water is critical in determining the oceanic heat flux into the ice because it separates the surface layer from the warm (>0°C) Atlantic water, as shown by Morison and Smith (1981) from observations on ice island T-3.

III. MODEL DEVELOPMENT

A. THE ICE GROWTH MODEL

The physical and dynamical properties of sea ice have been studied for many years but are still not completely understood. However, the most important aspects of sea ice have been extensively investigated and parameterizations and numerical models of varying degrees of sophistication have been developed to explain the behavior of sea ice. For this model only the most important physical processes will be included and will be treated in as simplified a manner as possible. The simplifications are not ad hoc but are based on the nature of the physical process involved and the extent it is understood. This method may lead to minor quantitative differences compared to more sophisticated models, but the goal here is to emphasize the role of mixed layer dynamics in limiting sea-ice growth. Hence, complexity attributed to other processes is minimized.

1. Longwave Radiation Fluxes

The first step is to linearize the Stefan-Boltzman Law near the freezing point to determine the upward radiant flux leaving the ice. Following Thorndike (1992) the Stefan-Boltzman Law can be written as:

$$F_{up} = \sigma T_{sfc}^4 = \sigma(T_f + T_{sfc})^4 \qquad (3.1)$$

where:

$\sigma = 5.7 \times 10^{-8}$ Wm^{-2}K^{-4} is the Stefan Boltzman constant
T_f=273 K is the freezing point of fresh water
T_{sfc} is the surface temperature in °C
F_{up} is the radient exitance in Wm^{-2}

Linearizing equation 3.1 leads to:

$$F_{up} = A + BT_{sfc} \qquad (3.2)$$

where
$A = \sigma(T_f)^4 = 320$ Wm^{-2}
$B = 4\sigma(T_f)^3 = 4.6$ Wm^{-2}K^{-1}

Using a surface temperature of -40°C with equation 3.1 gives a radiation

flux of 168 Wm^{-2} while equation 3.2 gives a radiation flux of 136 Wm^{-2} which is

a difference of 19%. The downward long wave radiation is paramaterized (

Maykut, 1986) as:

$$F_{LW} = \epsilon^* \sigma T_{air}^4 \qquad (3.3)$$

where:

ϵ^* is the effective emissivity of the atmosphere
σ is the Stefan Boltzman constant
T_{air} is the air temperature at 2 m and will be specified to simulate various
    atmospheric conditions

Maykut and Church (1973) developed an expression for ϵ^* based on

observations at Barrow, Alaska which is:

$$\epsilon^* = 0.7855(1 + 0.2232C^{2.75})$$

where:

C is the fractional cloud cover

2. Sensible Heat flux

Sensible heat flux in the atmospheric surface layer above the ice is the result of turbulent heat conduction between the atmosphere and the ice surface. Although the sensible heat flux is often ignored in climate studies of the central Arctic, it can be very important on shorter time scales. Figure 3.1 shows the variations of the sensible heat flux with ice thickness and season. In early March the sensible heat flux to the atmosphere exceeds 350 Wm^{-2} for 5 cm thick ice. The importance of the sensible heat flux decreases with increasing thickness of ice, and the sensible heat flux for 0.8 m thick ice is about 40 Wm^{-2}. The sensible heat flux has been paramaterized by Maykut (1986) as:

$$F_s = \rho_a c_{p_a} c_s \sqrt{u_{10}^2 + v_{10}^2} \ (T_{air} - T_{sfc}) \tag{3.4}$$

where

ρ_a is the density of air
c_{pa} is the specific heat of air
c_s is the bulk transfer coefficient for sensible heat
u_{10}, v_{10} is the wind speed at 10m

17

T_{air} is the air temperature at 2m
T_{sfc} is the temperature of the surface of the ice

Andreas (1987) has found the value for C_S to vary between 1.0 x 10⁻³ and 1.5 x 10⁻³. For this model the value of C_S will be fixed at 1.25 x 10⁻³. The air temperature at 2 meters will be specified to simulate various atmospheric conditions.

3. Conductive Heat Flux

After the summer melting season the surface of the ice begins to cool while the bottom of the ice remains near the freezing point of the adjacent seawater. When the ice surface becomes colder than the ice bottom an upward conduction of heat results.

This conductive heat flux is the amount of heat reaching the surface and depends on the temperature gradient across the ice and the thermal conductivity of the ice. Maykut and Untersteiner (1971) paramaterized the conductive heat flux as:

$$F_c = -K\frac{\partial T}{\partial z} \qquad (3.5)$$

Where:

F_c is the conductive heat flux
K is the thermal conductivity of ice
$\frac{\partial t}{\partial z}$ is the temperature gradient of the ice

18
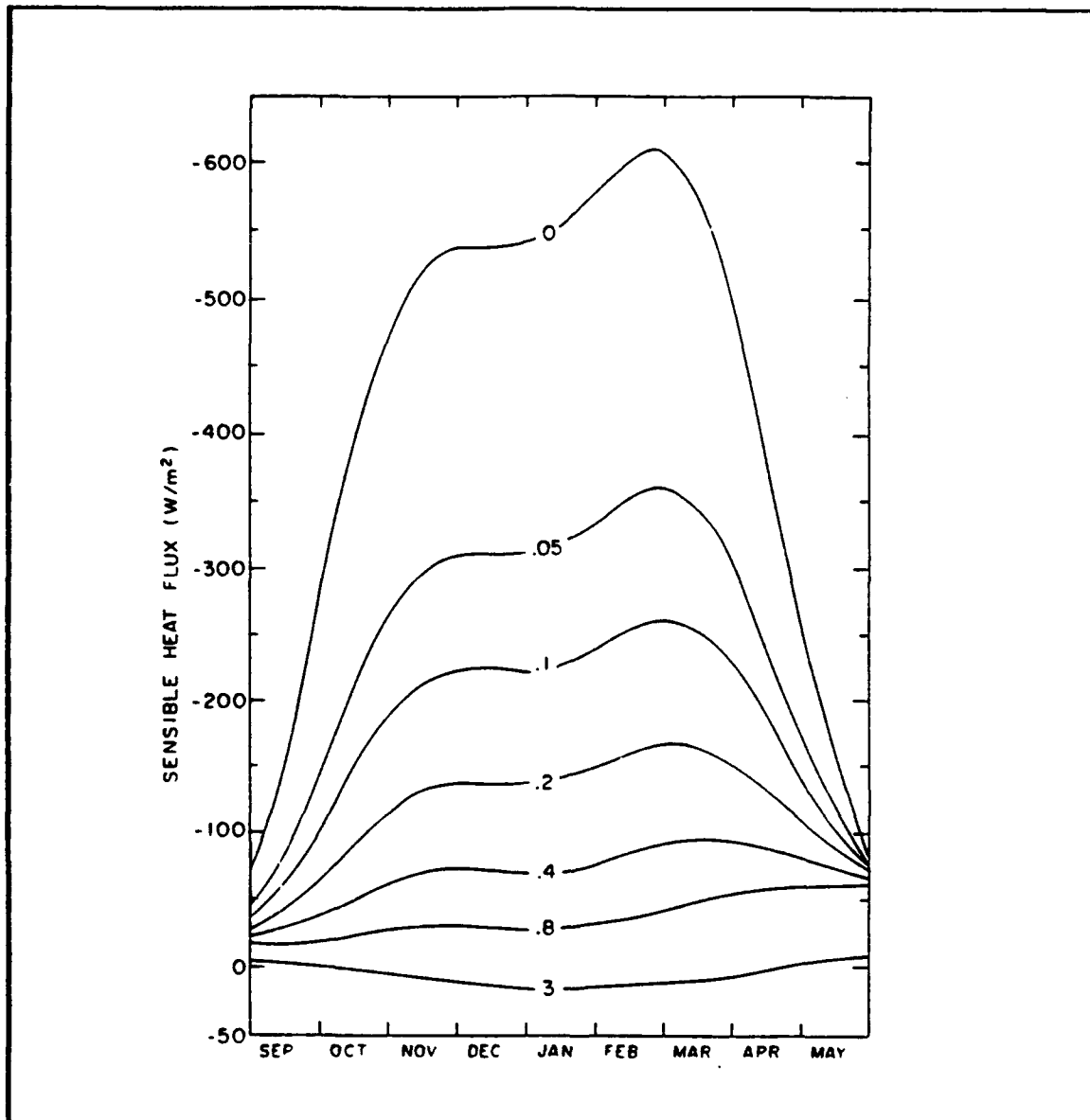
Figure 3.1 Seasonal Variation in the Sensible Heat Flux as a Function of Ice Thickness (m) (Maykut, 1986).

The thermal conductivity (K) of young ice can vary by as much as 50% (Maykut, 1986). However, following Thorndike (1992) K is considered to be constant of 2 $Wm^{-1} K^{-1}$. The temperature profile of the ice will be considered

linear, which Maykut (1978) showed to be a good approximation for young ice

and allows equation 3.5 to be written:

$$F_c = K \frac{T_f - T_{sfc}}{H} \qquad (3.6)$$

where:

H is the thickness of the ice
T_{sfc} is the temperature of the top of the ice
T_f is the temperature of the bottom of the ice using equation 3.7

a. Freezing point of sea water

Neglecting pressure effects, the freezing point temperature of

sea water is given by equation (15) (Millero and Leung, 1976):

$$T_f = a_0 s_1 + a_1 s_1^{3/2} + a_2 s_1^2 \qquad (3.7)$$

where:

a_0 = -0.0575
a_1 = 1.710523 x 10^{-3}
a_2 = -2.154996 x 10^{-4}
s_1 is the salinity of the mixed layer

4. Ice Motion

The equation of motion for sea ice balances ice acceleration against

air and water stresses, coriolis force, internal ice stress and the pressure

gradient force. Thorndike and Colony (1982) showed that over 70% of the

variance of the ice motion can be explained by the geostrophic wind and developed a free drift model that neglected the internal ice stresses. Hibler and Tucker (1979) show that in the short term the effects of the pressure gradient force is small compared to the coriolis force and wind and water stresses and is therefore neglected in this model. In any case, the geostrophic flow may be linearly separated from the force balance, and the equations for unsteady ice motion become:

$$\frac{\partial u_I}{\partial t} = f v_I + \frac{\tau_{x_{atm}} + \tau_{x_w}}{\rho_I H} \qquad (3.8)$$

$$\frac{\partial v_I}{\partial t} = -f u_I + \frac{\tau_{y_{atm}} + \tau_{y_w}}{\rho_I H} \qquad (3.9)$$

where:

u_I, v_I are the x and y components of ice velocity
f is the Coriolis Force
$\tau_{x_{atm}}$, $\tau_{y_{atm}}$ is the stress imparted on the ice from the wind.
τ_{x_w}, τ_{y_w} is the stress imparted on the ice from the ocean.
ρ_I is the density of the ice.
H is the thickness of the ice.

a.   Wind and Ocean stresses

The wind stress on the ice can be paramaterized as:

$$\tau_{x_{atm}} = \rho_a C_{D_a} (u_{10} - U) \sqrt{(u_{10} - u)^2 + (v_{10} - v)^2} \qquad (3.10)$$

21

$$\tau_{y_{ain}} = \rho_a C_{D_a}(V_{10}-V)\sqrt{(u_{10}-u)^2+(V_{10}-V)^2} \qquad (3.11)$$

While the ocean stress on the ice can be parameterized as:

$$\tau_{x_w} = \rho_w C_{D_i}(u_i-u_w)\sqrt{(u_i-u_w)^2+(v_i-v_w)^2} \qquad (3.12)$$

$$\tau_{y_w} = \rho_w C_{D_i}(v_i-v_w)\sqrt{(u_i-u_w)^2+(v_i-v_w)^2} \qquad (3.13)$$

where:

ρ_a is the density of air
ρ_w is the density of sea water
C_{D_a} is the ice surface drag coefficient
C_{D_i} is the ice bottom drag coefficient
u_{10}, v_{10} are the x and y components of the wind speed at 10m
u_i, v_i are the x and y components of the ice velocity
u_w, v_w are the x and y components of the ocean mixed layer velocity

Guest and Davidson (1991) measured the surface drag coefficient (C_{D_a}) of various ice types. For this model a constant value of 2.3 x 10^{-3} will be used for C_{D_a} which corresponds to Guest and Davidson's median value for smooth young ice. McPhee (1990) emphasized the difficulty in determining a bottom drag coefficient and the wide range of values of C_{D_w} that have been obtained. However, this model uses a constant value of 5.4 x 10^{-3} for the bottom drag coefficient following McPhee (1979).

5. Oceanic Heat Flux

The ocean heat flux is the result of warmer water being entrained into the mixed layer due to turbulent mixing and is paramaterized by Chu and Garwood (1988) as:

$$F_w = -\rho_w \, c_{\rho_w} \, w_e \, \Delta T \qquad (3.14)$$

where:

F_w is the ocean heat flux due to entrainment
ρ_w is the density of sea water
w_e is the entrainment rate
ΔT is the temperature difference between the ocean mixed layer and the water below.

The entrainment rate w_e is given in equation 3.28 and is determined by the one-dimensional mixed layer model which is discussed in section B of Chapter III.

6. Ice Growth

The rate of ice growth or melting will be determined by the balance of fluxes into and out of the ice. Latent heat is released at the bottom of the ice by changing water into ice when the conductive heat flux upward into the ice exceeds the ocean heat flux upward into the mixed layer. The ice will melt if the ocean heat flux is greater than the conductive heat flux (Thorndike, 1992). The latent heat flux due to the change in ice thickness is given as:

23

$$F_I = L \frac{dH}{dt}$$

Where:

F$_i$ is the latent heat flux due to change in ice thickness
L is the latent heat of fusion for ice
dH/dt is the rate of change in ice thickness

The latent heat of fusion is considered to be constant at 3×10^8 J m^{-3}

The balance of heat fluxes is represented in Figure 3.2. Summing

the heat fluxes at the surface of the ice yields:

$$F_{LW} + F_c + F_s = F_{up} \qquad (3.15)$$

and summing the heat fluxes at the bottom of the ice yields:

$$L \frac{dH}{dt} = F_c - F_w \qquad (3.16)$$

Using equations 3.2, 3.4 and 3.6 with equation 3.15 gives:

$$F_{LW} + K \frac{(T_f - T_{sfc})}{H} = \rho_a C_{p_a} C_s \sqrt{u_{10}^2 + v_{10}^2} \, (T_{sfc} - T_a) + A + BT_{sfc} \qquad (3.17)$$

Using equations 3.6 and 3.14 with equation 3.16 gives:

$$L\frac{dH}{dT} = K\frac{(T_f - T_{sfc})}{H} + \rho_w c_p w_e \, \Delta T \tag{3.18}$$

Solving equation 3.17 for the surface temperature yields:

$$T_{sfc} = \frac{F_{LW} - A + \rho_a c_{p_a} c_s \sqrt{u_{10}^2 + v_{10}^2}\, T_a}{B + \rho_a c_{p_a} c_s \sqrt{u_{10}^2 + v_{10}^2} + \dfrac{K}{H}} + \frac{KT_f}{BH + \rho_a c_{p_a} c_s \sqrt{u_{10}^2 + v_{10}^2}\, H + K} \tag{3.19}$$
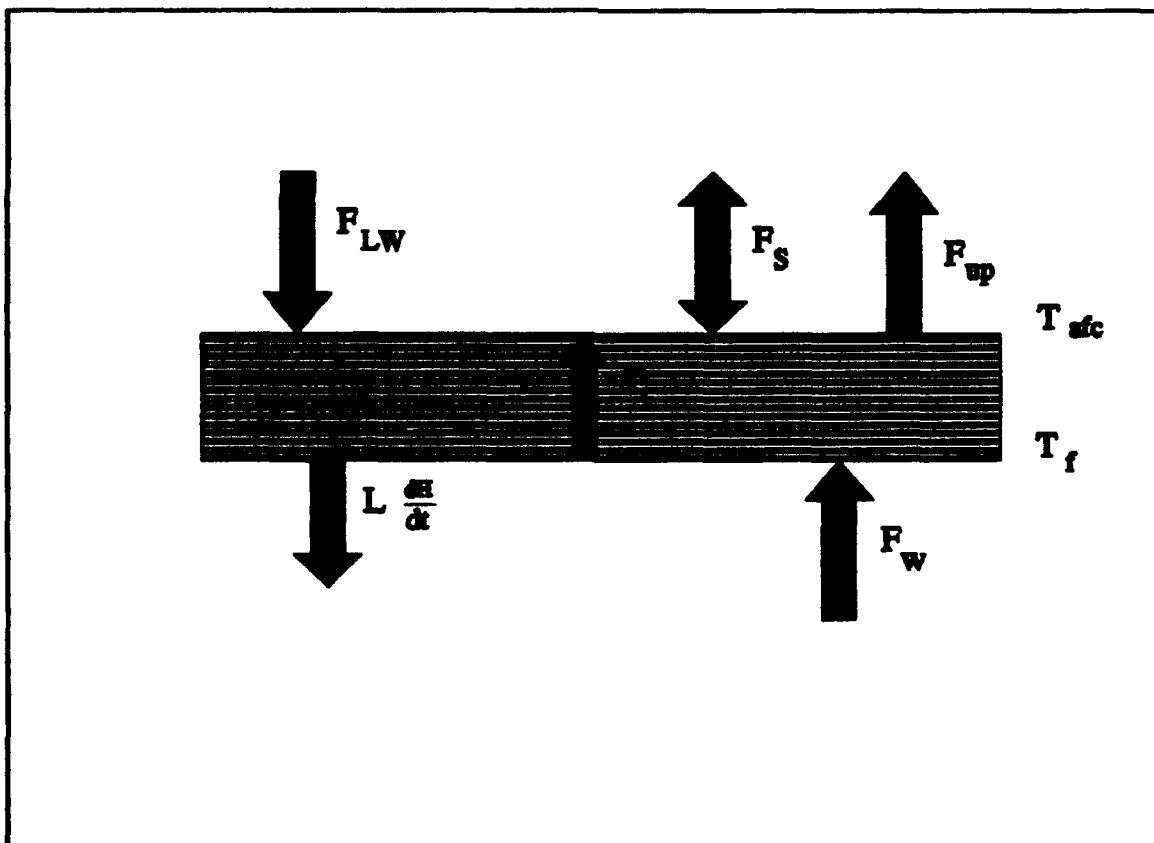
Figure 3.2   The Heat Fluxes That Determine The Ice Growth and Temperature (from Thorndike, 1992)

25

Finally, solving equation 3.18 for ice growth gives:

$$\frac{dH}{dt} = K\frac{(T_f - T_{sfc})}{LH} + \frac{1}{L}(\rho_w c_{p_w} W_e \, \Delta T)$$ (3.20)

B. OCEAN MIXED LAYER MODEL

The mixed layer model used here is a tunable, one dimensional Kraus and Turner (1967) type mixed layer model. The model assumptions following Niiler and Kraus (1977) are:

1. The mean temperature, salinity and horizontal velocity are assumed to be uniform within the mixed layer.

2. On the depth and time scales of the model, temperature, salinity and horizontal velocity discontinuities can exist across the lower boundary of the mixed layer.

3. Temperature changes associated with frictional dissipation are neglected.

4. Wind and ice stresses, turbulent kinetic energy and viscous dissipation are considered to be horizontally uniform.

Additional assumptions are:

5. The temperature of the mixed layer remains at the freezing point, thus not allowing storage of heat by the mixed layer and neglecting the effect of supercooling at the water surface.

6. Loss of turbulence to internal waves is ignored.

7. Only the case of deepening mixed layer will be considered at the present time.

26

1. Turbulent Kinetic Energy Equation

The model is derived from the turbulent kinetic energy (TKE) equation, equation 3.21 (Garwood, 1977):

$$\frac{1}{2}\frac{\partial\overline{(u'^2+v'^2+w'^2)}}{\partial t} = -\left[\overline{u'w'}\frac{\partial\overline{u}}{\partial z} + \overline{v'w'}\frac{\partial\overline{v}}{\partial z}\right] - \frac{\overline{w'\rho'}}{\rho_0}g - \frac{\partial}{\partial z}\left[\overline{w'\left(\frac{\overline{u'^2+v'^2+w'^2}}{2} + \frac{\overline{\rho'}}{\rho_0}\right)}\right] - \epsilon$$

(3.21)

I   II   III   IV   V

From Stull (1988):

- Term I is the local storage tendency of TKE.

- Term II is the shear production of TKE due to vertical shear of the horizontal mean flow.

- Term III is the buoyant production or consumption of TKE depending on whether the buoyancy flux is positive (upwards) or negative (downward).

- Term IV is turbulent transport of TKE by turbulent eddies and the pressure transport of TKE due to pressure perturbations and can be positive or negative.

- Term V is the viscous dissipation of TKE due to the conversion of TKE into heat and will always be negative.

The TKE budget of the ocean can be assumed to be in steady state because of the very short time scale for dissipation. This allows Term I of equation 3.21 to be assumed equal to zero.

27

2. Vertically Integrated TKE Equation

Equation 3.21 is now vertically integrated over the depth of the mixed layer and, following Claes (1990) , gives the bulk form of the TKE equation:

$$0 = \frac{c_1 u_*^3}{h} + \left[\alpha g \overline{T'w'}(0) - \beta g \overline{s'w'}(0)\right] + \left[\alpha g \overline{T'w'}(-h) - \beta g \overline{s'w'}(-h)\right] \quad (3.22)$$

$$\qquad\qquad\quad \text{I} \qquad\qquad\qquad\qquad \text{II} \qquad\qquad\qquad\qquad\qquad \text{III}$$

where:

  c_1 is a constant of proportionality
  u_* is the water surface friction velocity
  h is the depth of the mixed layer
  α is the thermal expansion coefficient
  β is the salinity contraction coefficient
  g is gravity
  $\overline{T'w'}(0)$ is the temperature flux at the top of the mixed layer

  $\overline{s'w'}(0)$ is the salinity flux at the top of the mixed layer

  $\overline{T'w'}(-h)$ is the temperature flux at the base of the mixed layer

  $\overline{s'w'}(-h)$ is the salinity flux at the bottom of the mixed layer

Because the temperature of the mixed layer is kept at the freezing point, any addition or loss of heat will go to melting or freezing ice. Hence the water surface temperature flux $\alpha g \overline{T'w'}(0)$ is equal to zero.

a. Ice stress and TKE transport

Term I in equation 3.22 represents the shear production minus viscous dissipation integrated over the full depth of the mixed layer. The constant c_1 is reduced exponentially on a vertical scale of u_*/f (Chu and Garwood, 1988) and is approximately:

$$c_1 \approx 2e^{(-fh/u_*)}$$

where:

    f is the coriolis parameter
    h is the depth of the mixed layer
    u_* is the water surface friction velocity.

c_1 can be tuned to match observations. The friction velocity (u_*) is represented by:

$$U_* = \left[\frac{\tau_{x_i}^2 + \tau_{y_i}^2}{\rho_w}\right]^{1/2}$$

where:
    τ_{x_i}, τ_{y_i} are the stresses imparted on the water from the ice .
    ρ_w is the density of the sea water.

The ice stresses τ_{x_i} and τ_{y_i} are equal but opposite in sign to the stress imparted on the ice from the water, given in equations 3.12 and 3.13.

b. Buoyancy fluxes

The buoyancy flux at the surface of the mixed layer will be determined by the salinity flux at the top of the mixed layer due to ice formation

29

or melting, while the buoyancy flux at the base of the mixed layer will be determined by the heat and salinity fluxes due to entrainment of water from below the mixed layer.

(1) *Surface buoyancy flux.* The $\overline{s'w'}(0)$ term of equation 3.22 is the surface salinity flux that results from the freezing or melting of ice and is:

$$\overline{s'w'}(0) = \frac{\rho_i}{\rho_w}(s_i - s_1)\frac{dH}{dt} \tag{3.23}$$

where:
  ρ_i is the density of the ice
  ρ_w is the density of the sea water
  s_1 is the salinity of the mixed layer
  s_i is the salinity of the ice
  dH/dt is the growth rate of the ice

Term II of equation 3.22 is the surface buoyancy flux $\overline{b'w'}(0)$ and using equation 3.23 can be written as:

$$\overline{b'w'}(0) = \beta g\frac{\rho_i}{\rho_w}(s_1 - s_i)\frac{dH}{dt} \tag{3.24}$$

(2) *Buoyancy flux at the base of the mixed layer.* The $\overline{T'w'}(-h)$ and $\overline{s'w'}(-h)$ terms of equation 3.22 are the heat and salinity fluxes at the base of the mixed layer that result from the entrainment of water, with different temperature and salinity, from below the mixed layer . Garwood

30

(1977) develops the jump condition for the turbulent fluxes at the base of the mixed layer by integrating across the entrainment zone and assuming a negligible amount of heat stored in the entrainment zone. This allows the temperature flux at the base of the mixed layer to be written as:

$$\overline{T'w'}(-h) = -\Delta T w_e \qquad (3.25)$$

where:

$$\Delta T = T_f - T_2$$

ΔT is the temperature jump between the mixed layer temperature and the deep   water temperature

T_f is the mixed layer temperature which is at the freezing point
T_2 is the deep water temperature

and the salinity flux to be written as:

$$\overline{s'w'}(-h) = -\Delta s w_e \qquad (3.26)$$

where:

$$\Delta s = s_1 - s_2$$

where :

Δs is the salinity jump between the mixed layer salinity and the deep water salinity.
     s_1 is the mixed layer salinity

31

s_2 is the deep ocean salinity

w_e is the entrainment velocity

Term III of equation 3.22 is the buoyancy flux $\overline{b'w'}(-h)$ at the base of the mixed layer. Using equations 3.25 and 3.26 can be written as:

$$\overline{b'w'}(-h) = \alpha g \overline{T'w'}(-h) - \beta g \overline{s'w'}(-h) \qquad (3.27)$$

with :

$$\Delta b = \alpha g \Delta T - \beta g \Delta s$$

Δb is the buoyancy jump between the mixed layer and the deep water

3.   Entrainment Velocity

The entrainment velocity can be obtained from equation 3.22

combined with equations 3.24 and 3.27 and an added tuning constant c_2, which

is a function of stability, to yield:

$$0 = \frac{c_1 u_*^3}{h} + c_2 \beta g \frac{\rho_I}{\rho_w}(s_1 - s)\frac{dH}{dt} - \Delta b w_e \qquad (3.28)$$

Solving equation 3.28 for the entrainment velocity, W_e gives:

$$w_e = \frac{1}{\Delta b}\left[\frac{c_1 u_*^3}{h} + c_2 \beta g \frac{\rho_I}{\rho_w}(s_1 - s)\frac{dH}{dt}\right] \qquad (3.29)$$

or

32

$$W_e = \frac{1}{\alpha g \Delta T - \beta g \Delta s}\left[\frac{c_1 u_*^3}{h} + c_2 \beta g \frac{\rho_i}{\rho_w}(s_1 - s_i)\frac{dH}{dt}\right] \qquad (3.29)$$

4. Mixed Layer Motion

The equations of motion for the mixed layer are determined by integrating the mean momentum equation across the depth of the mixed layer (Garwood, 1977), resulting in equations 3.30 and 3.31

$$\frac{\partial u_w}{\partial t} = f v_w + \frac{\tau_{xi}}{\rho_w h} - \frac{u_w W_e}{h} - c_3 u_w \qquad (3.30)$$

$$\frac{\partial v_w}{\partial t} = -f u_w + \frac{\tau_{yi}}{\rho_w h} - \frac{v_w W_e}{h} - c_3 v_w \qquad (3.31)$$

where:

u_w, v_w are the horizontal velocities of the mixed layer
f is the coriolis force
h is the depth of the mixed layer
ρ_w is the density of the mixed layer
w_e is the entrainment rate
τ_{xi}, τ_{yi} are the stresses imparted on the mixed layer by the ice motion
c_3 is a linear damping constant.

The linear damping term (c_3) has been added to equations 3.30 and 3.31 to model the momentum dispersion effect (Pollard and Millard, 1970) and can be tuned to match observations. Typically, $c_3 \approx (2\ days)^{-1}$.

5. Mixed Layer Salinity

The salinity of the mixed layer will vary as a result of the salinity fluxes given by equations 3.2 and 3.26. The salinity equation is determined by integrating the mean salinity equation across the depth of the mixed layer and is given as:

$$\frac{\partial s_1}{\partial t} = \frac{1}{h}\left[\frac{\rho_I}{\rho_w}(s_1 - s_i)\frac{dH}{dt} - w_e\Delta s \right] \qquad (3.32)$$

IV. MODEL RESULTS

A. MODEL INITIAL CONDITIONS

The closely coupled nature of ice growth with atmospheric and oceanic forcings does not lend itself to a sensitivity study where only one parameter is varied while all others are held constant. However, by varying initial conditions and boundary conditions in the model, the sensitivity of the model to the various parameters can be determined. The model boundary conditions are the air temperature, wind speed, and cloudiness. The initial conditions are ice velocity, mixed layer velocity, initial mixed layer salinity, the deep layer temperature, the deep layer salinity and the initial mixed layer depth. Table 4.1 lists the case solutions and the parameter that was varied. Output for all model cases is shown in the appendix. The first case is the standard against which the effect of the variations will be considered and is based on the temperature and salinity profiles shown in Figure 2.1. For all runs the initial velocity of the ice and mixed layer are kept constant as is the cloudiness. One of the major goals of this research is to study the variation in the oceanic heat flux and its effect on the growth rate of ice.

1. VARYING WIND SPEED

Calm winds were not considered in this study, although this may be an important situation. When the winds calm, the mixed layer will shallow, entrainment will cease, and there will be no ocean heat flux into the ice.

The standard case wind speed is chosen to be approximately 7ms^{-1} while in case 2 the wind speed is doubled to 14ms^{-1}. The increased wind speed has two effects on the ice growth rate. First, the sensible heat flux is increased which decreases the surface temperature of the ice. Second, as can be seen from equation 3.29, the mechanical mixing (u_*) term will increase eight-fold when the wind speed (and u_*) is increased by a factor of two. This leads to a large entrainment rate (w_e) and a heat flux that exceeds the conductive heat flux (F_c) in less than four days and begins to melt the ice.

2. VARYING AIR TEMPERATURE

When the air temperature is increased from $-30.0°$ C to $-10.0°$ C, the incoming net longwave radiation is increased to 220 Wm^{-2}. This increased heat into the ice increases the surface temperature of the ice to the point that the sensible heat flux becomes positive which also leads to a warmer surface temperature. The warmer surface temperature decreases the conductive heat flux and slows the growth rate of the ice. The slower ice growth has two effects on the ocean heat flux. First, the surface buoyancy flux is decreased which slows the entrainment rate (w_e) and second, there is less salt being ejected into the mixed layer. Since the freezing temperature is determined by the mixed

layer salinity, the temperature jump (ΔT) is also decreased. This results in a lower ocean heat flux, however, the ocean heat flux is actually a larger percentage of the conductive heat flux in this case.

3.   VARYING THE ICE THICKNESS

Decreasing the initial ice thickness (H) to 0.05 m causes the surface temperature to increase but still results in almost doubling the conductive heat flux (F_c). This large conductive heat flux rapidly decreases as the ice thickens because the temperature gradient across the ice changes much more slowly than does the change in ice thickness. The rapid ice growth causes an increase in the entrainment rate and the ocean heat flux. The increase in entrainment rate manifests itself in the increased depth of the mixed layer (h).

Increasing the initial ice thickness (H) to 2m allows the surface temperature to decrease but results in almost a 50% decrease in the conductive heat flux and a slowing in the ice growth rate. This slower ice growth rate results in a slower change in the buoyancy jump (Δb) between the mixed layer and the deep layer because the mixed layer is now fresher than in the standard case.

4.   VARYING THE MIXED LAYER DEPTH

Decreasing the initial mixed layer depth (h) sharply increases the entrainment rate for two reasons. First, the mechanical mixing is inversely proportional to the mixed layer depth (h) times Δb. Second, the surface

37

buoyancy flux is increased due to the rapid increase in mixed layer salinity which is also inversely proportional to the mixed layer depth as shown in equation 3.32. Increasing the initial mixed layer depth to 45m likewise decreases the ocean heat flux as the entrainment rate (w_e) becomes proportionally smaller to the entrainment rate in the standard case.

5. VARYING THE DEEP LAYER SALINITY

Increasing the deep layer salinity (s_2) to 31.25 psu reduces the entrainment velocity (w_e) because the deep water is now denser and requires more work to lift it into the mixed layer. The salinity jump Δs does decrease at a more rapid rate due to the increased ice growth, but it is not enough to offset the larger initial Δs.

Decreasing the deep layer salinity to 30.35 psu results in a large increase in the entrainment rate (w_e) because of the decreased buoyancy jump (Δb). The decrease in the ice growth and consequent decrease in the surface buoyancy flux is very small compared to the increased entrainment rate.

6. VARYING THE DEEP LAYER TEMPERATURE

Increasing the deep layer temperature (T_2) to -1.2°C increases the ocean heat flux by increasing the temperature jump (ΔT). However, this produces only a slight change in the entrainment velocity because the thermal

38

expansion coefficient (α) is so much smaller than the salinity contraction coefficient (β).

The effect of decreasing T_2 so that the ocean is essentially isothermal is not shown here, but would result in a vanishing ocean heat flux.

7. VARYING THE MIXED LAYER SALINITY.

Increasing the initial mixed layer salinity (s_1) to 30.35 psu not only decreases the salinity jump (Δs) but it also increases the temperature jump (ΔT) which leads to larger entrainment rates (w_e) and consequently a larger ocean heat flux (F_w). A decrease in salinity leads to a similar but opposite result, although this is not shown here.

TABLE 4.1   STANDARD RUN VALUES AND VARIED PARAMETER VALUES

RUN #	PARAMETER VARIED	PARAMETER VALUE
Run 1	Standard Case	T_a = -30.0°C u_{10}= 5.0 ms^{-1} v_{10}= 5.0 ms^{-1} s_1 = 29.9 psu s_2 = 30.8 psu T_2=-1.4°C H = 1.0 m h =30.0 m
Run 2	Wind Speed	u_{10} = 10.0 ms^{-1} v_{10} = 10.0 ms^{-1}
Run 3	Air Temperature	T_a = -10.0°C
Run 4	Ice Thickness	H = 0.5 m
Run 5	Ice Thickness	H = 2.0 m
Run 6	Mixed Layer Depth	h = 15.0 m
Run 7	Mixed Layer Depth	h = 45.0 m
Run 8	Salinity Jump, Δs	s_2 = 31.25 psu
Run 9	Salinity Jump, Δs	s_2 = 30.35 psu
Run 10	Temperature Jump, ΔT	T_2 = -1.2°C
Run 11	Salinity Jump, Δs Temperature Jump, ΔT	s_1 = 30.35 psu

V. CONCLUSIONS

A. SUMMARY

This study has investigated the effects of mixed layer dynamics on the growth of sea ice using a coupled ice-mixed layer model. The ice is modeled as undeformed ice with a linear temperature profile and constant conductivity. The ocean is modeled as a one dimensional, two layer system. Important prognostic variables include ice thickness, mixed layer salinity, and mixed layer depth. As long as ice is present, the mixed layer temperature is held at the freezing point, which is dependent upon the mixed layer salinity. The surface temperature of the ice varies in response to the net surface heat fluxes.

Model solutions revealed the response of the model to initial conditions, varying one parameter at a time. These parameters included wind stress, air temperature, mixed layer depth, ice thickness, and temperature and salinity jumps between the mixed layer and deep layer. The model simulations showed:

- There is a negative feed back between the ice growth rate and the mixed layer entrainment rate.

- Increasing wind stress leads to a rapid increase in the entrainment rate into the mixed layer and an upward ocean flux that exceeds the conductive heat flux.

41

- The mixed layer entrainment rate is strongly influenced by the ice growth rate through its effects on the surface buoyancy flux, mixed layer temperature and salinity and subsequent effect on the buoyancy jump Δb.

- Varying the deep layer salinity has a greater effect on the ocean heat flux than does varying the deep layer temperature.

- Increasing the mixed layer salinity leads to a large increase in the ocean heat flux through the combined effects of increasing the temperature jump ΔT and decreasing the buoyancy jump Δb.

- Increasing the mixed layer depth decreases the entrainment rate by decreasing the effects of wind stress and decreasing the surface buoyancy flux. Decreasing the mixed layer depth increases the entrainment rate for the same reasons.

- The large range of heat fluxes precludes modelling the heat flux as a constant or using more simplified physics to determine the ocean heat flux.

B. RECOMMENDATIONS

The model shows the importance of mixed layer dynamics on ice growth during the freezing cycle and under active mixed layer deepening. This research has highlighted several areas of improvement and areas of further study:

- Incorporating the three dimensional Naval Postgraduate School mixed layer model (Adamec et al., 1981) with the ice growth model to allow for deepening and shallowing of the mixed layer and advection.

- The effect of storms and varying wind stresses on the ocean heat flux.

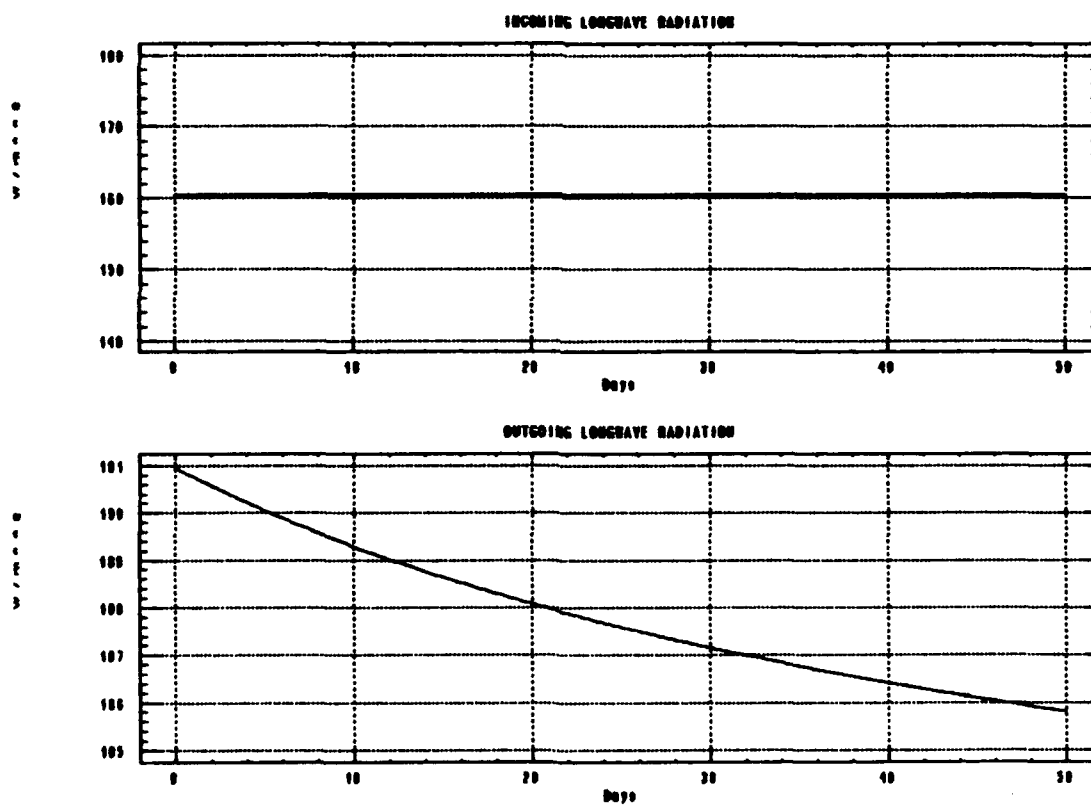- Determination of the equilibrium thickness of sea ice through an entire year.

42

APPENDIX   MODEL RUN RESULTS

Run 1:

INITIAL CONDITIONS :

u_i = 0.1 ms⁻¹ u_{10} = 5.0 ms⁻¹
s_i = 9.0 psu v_{10} = 5.0 ms⁻¹
v_i = 0.1 ms⁻¹ T_a = - 30.0° C
u_w = 3.0x10⁻³ ms⁻¹ T_2 = - 1.4° C
v_w = 3.0x10⁻³ ms⁻¹ s_2 = 30.8 psu
s_1 = 29.9 psu
H = 1.0 m
h = 30.0 m

INCOMING LONGWAVE RADIATION

OUTGOING LONGWAVE RADIATION

43

APPENDIX   MODEL RUN RESULTS

Run 1:

INITIAL CONDITIONS :

$u_i = 0.1 \text{ ms}^{-1}$ $u_{10} = 5.0 \text{ ms}^{-1}$

$s_i = 9.0 \text{ psu}$ $v_{10} = 5.0 \text{ ms}^{-1}$

$v_i = 0.1 \text{ ms}^{-1}$ $T_a = -30.0° \text{ C}$

$u_w = 3.0 \times 10^{-3} \text{ ms}^{-1}$ $T_2 = -1.4° \text{ C}$

$v_w = 3.0 \times 10^{-3} \text{ ms}^{-1}$ $s_2 = 30.8 \text{ psu}$

$s_1 = 29.9 \text{ psu}$

$H = 1.0 \text{ m}$

$h = 30.0 \text{ m}$

INCOMING LONGWAVE RADIATION

OUTGOING LONGWAVE RADIATION

43

CONDUCTIVE HEAT FLUX

SENSIBLE HEAT FLUX

OCEAN HEAT FLUX

Days

44

ENTRAINMENT VELOCITY

TEMPERATURE DIFFERENCE (T1-T2)

SALINITY DIFFERENCE (S1-S2)

45

SURFACE TEMPERATURE

ICE THICKNESS

MIXED LAYER DEPTH

Run 2:

INITIAL CONDITIONS :

u_i = 0.1 ms^{-1} u_{10} = 10.0 ms^{-1}
s_i = 9.0 psu v_{10} = 10.0 ms^{-1}
v_i = 0.1 ms^{-1} T_a = - 30.0° C
u_w = 3.0x10^{-3} ms^{-1} T_2 = - 1.4° C
v_w = 3.0x10^{-3} ms^{-1} s_2 = 30.8 psu
s_1 = 29.9 psu
H = 1.0 m
h = 30.0 m

CONDUCTIVE HEAT FLUX

SENSIBLE HEAT FLUX

OCEAN HEAT FLUX

48

ENTRAINMENT VELOCITY

20

16

12

8

4

0

0   10   20   30   40   50
Days

TEMPERATURE DIFFERENCE (T1-T2)

-0.23

-0.24

-0.25

-0.26

-0.27

-0.28

0   10   20   30   40   50
Days

SALINITY DIFFERENCE (S1-S2)

-0.1

-0.3

-0.5

-0.7

-0.9

0   10   20   30   40   50
Days

49

SURFACE TEMPERATURE

ICE THICKNESS

MIXED LAYER DEPTH

50

Run 3:

$u_i = 0.1\ ms^{-1}$

$s_i = 9.0\ psu$

$v_i = 0.1\ ms^{-1}$

$u_w = 3.0 \times 10^{-3}\ ms^{-1}$

$v_w = 3.0 \times 10^{-3}\ ms^{-1}$

$s_1 = 29.9\ psu$

$H = 1.0\ m$

$h = 30.0\ m$

$u_{10} = 5.0\ ms^{-1}$

$v_{10} = 5.0\ ms^{-1}$

$T_a = -10.0^\circ\ C$

$T_2 = -1.4^\circ\ C$

$s_2 = 30.8\ psu$

INCOMING LONGWAVE RADIATION

OUTGOING LONGWAVE RADIATION

51

CONDUCTIVE HEAT FLUX

SENSIBLE HEAT FLUX

OCEAN HEAT FLUX

52

ENTRAINMENT VELOCITY

TEMPERATURE DIFFERENCE (T1-T2)

SALINITY DIFFERENCE(S1-S2)

53

SURFACE TEMPERATURE

ICE THICKNESS

MIXED LAYER DEPTH

Run 4:

$u_i = 0.1 \text{ ms}^{-1}$ $u_{10} = 5.0 \text{ ms}^{-1}$

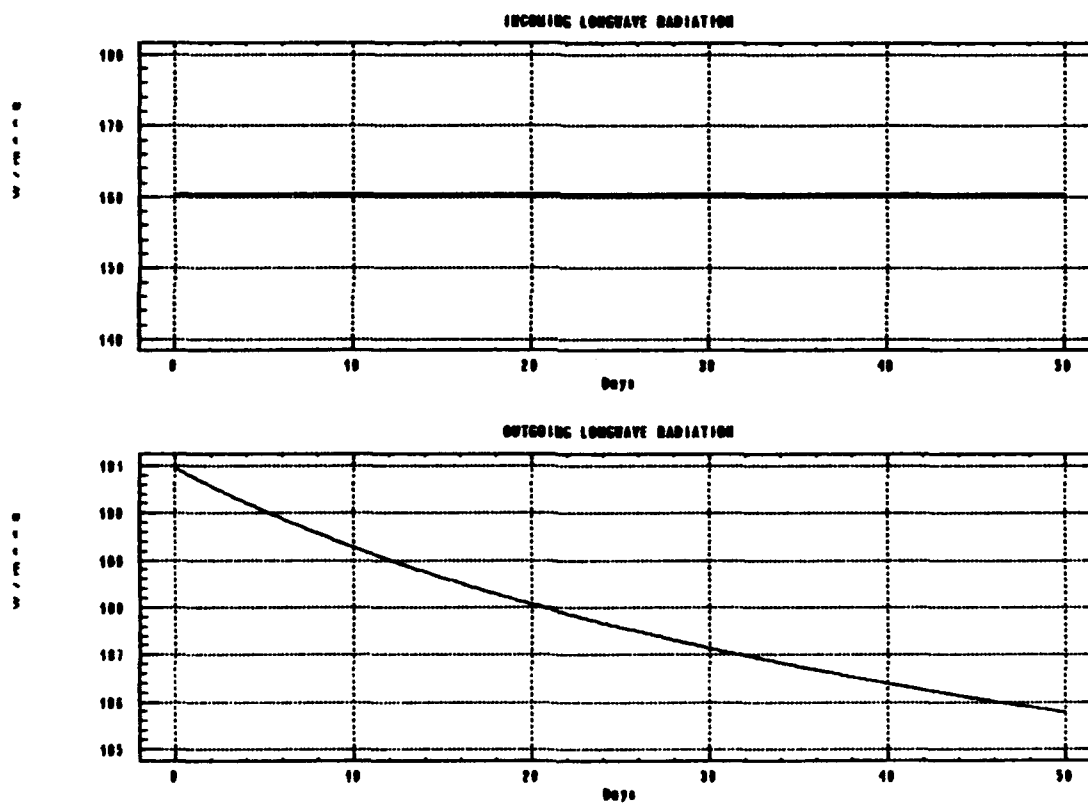$s_i = 9.0 \text{ psu}$ $v_{10} = 5.0 \text{ ms}^{-1}$

$v_i = 0.1 \text{ ms}^{-1}$ $T_a = -30.0^\circ \text{ C}$

$u_w = 3.0 \times 10^{-3} \text{ ms}^{-1}$ $T_2 = -1.4^\circ \text{ C}$

$v_w = 3.0 \times 10^{-3} \text{ ms}^{-1}$ $s_2 = 30.8 \text{ psu}$

$s_1 = 29.9 \text{ psu}$

$H = 0.5 \text{ m} \quad h = 30.0 \text{ m}$

55

CONDUCTIVE HEAT FLUX

SENSIBLE HEAT FLUX

OCEAN HEAT FLUX

56

ENTRAINMENT VELOCITY

TEMPERATURE DIFFERENCE (T1-T2)

SALINITY DIFFERENCE (S1-S2)

57

SURFACE TEMPERATURE

ICE THICKNESS

MIXED LAYER DEPTH

58

Run 5:

INITIAL CONDITIONS :

u_i = 0.1 ms^{-1} u_{10} = 5.0 ms^{-1}
s_i = 9.0 psu v_{10} = 5.0 ms^{-1}
v_i = 0.1 ms^{-1} T_a = - 30.0° C
u_w = 3.0x10^{-3} ms^{-1} T_2 = - 1.4° C
v_w = 3.0x10^{-3} ms^{-1} s_2 = 31.5 psu
s_1 = 30.9 psu
H = 2.0 m
h = 30.0 m

INCOMING LONGWAVE RADIATION

OUTGOING LONGWAVE RADIATION

CONDUCTIVE HEAT FLUX

SENSIBLE HEAT FLUX

OCEAN HEAT FLUX

60

ENTRAINMENT VELOCITY

TEMPERATURE DIFFERENCE (T1-T2)

SALINITY DIFFERENCE (S1-S2)

61

SURFACE TEMPERATURE

ICE THICKNESS

MIXED LAYER DEPTH

Run 6:

INITIAL CONDITIONS :

u_i = 0.1 ms^{-1} u_{10} = 5.0 ms^{-1}
s_i = 9.0 psu v_{10} = 5.0 ms^{-1}
v_i = 0.1 ms^{-1} T_a = - 30.0° C
u_w = 3.0x10^{-3} ms^{-1} T_2 = - 1.4° C
v_w = 3.0x10^{-3} ms^{-1} s_2 = 30.8 psu
s_1 = 29.9 psu
H = 1.0 m
h = 15.0 m

INCOMING LONGWAVE RADIATION

OUTGOING LONGWAVE RADIATION

CONDUCTIVE HEAT FLUX

SENSIBLE HEAT FLUX

OCEAN HEAT FLUX

64

ENTRAINMENT VELOCITY

TEMPERATURE DIFFERENCE (T1-T2)

SALINITY DIFFERENCE (S1-S2)

65

SURFACE TEMPERATURE

ICE THICKNESS

MIXED LAYER DEPTH

66

Run 7:

$u_i = 0.1\ ms^{-1}$ $u_{10} = 5.0\ ms^{-1}$

$s_i = 9.0\ psu$ $v_{10} = 5.0\ ms^{-1}$

$v_i = 0.1\ ms^{-1}$ $T_a = -30.0°\ C$

$u_w = 3.0\times10^{-3}\ ms^{-1}$ $T_2 = -1.4°\ C$

$v_w = 3.0\times10^{-3}\ ms^{-1}$ $s_2 = 31.5\ psu$

$s_1 = 30.9\ psu$

$H = 1.0\ m$

$h = 45.0\ m$

67

CONDUCTIVE HEAT FLUX

w / m**2

54					
50					
45					
42					
30					
34					

0   10   20   30   40   50

Days

SENSIBLE HEAT FLUX

w / m**2

-8					
-11					
-14					
-17					
-20					
-23					

0   10   20   30   40   50

Days

OCEAN HEAT FLUX

w / m**2

1.55					
1.45					
1.35					
1.25					
1.15					
1.05					
0.95					

0   10   20   30   40   50

Days

68

ENTRAINMENT VELOCITY

TEMPERATURE DIFFERENCE (T1-T2)

SALINITY DIFFERENCE (S1-S2)

69

SURFACE TEMPERATURE

ICE THICKNESS

MIXED LAYER DEPTH

70

Run 8:

$u_l = 0.1\ ms^{-1}$ $u_{10} = 5.0\ ms^{-1}$
$s_l = 9.0\ psu$ $v_{10} = 5.0\ ms^{-1}$
$v_l = 0.1\ ms^{-1}$ $T_a = -30.0^\circ\ C$
$u_w = 3.0 \times 10^{-3}\ ms^{-1}$ $T_2 = -1.4^\circ\ C$
$v_w = 3.0 \times 10^{-3}\ ms^{-1}$ $s_2 = 31.25\ psu$
$s_l = 29.9\ psu$
$H = 1.0\ m$
$h = 30.0\ m$

71

CONDUCTIVE HEAT FLUX

SENSIBLE HEAT FLUX

OCEAN HEAT FLUX

ENTRAINMENT VELOCITY

TEMPERATURE DIFFERENCE (T1-T2)

SALINITY DIFFERENCE (S1-S2)

73

SURFACE TEMPERATURE

ICE THICKNESS

MIXED LAYER DEPTH

74

Run 9:

INITIAL CONDITIONS :

$u_i = 0.1\ ms^{-1}$ $u_{10} = 5.0\ ms^{-1}$
$s_i = 9.0\ psu$ $v_{10} = 5.0\ ms^{-1}$
$v_i = 0.1\ ms^{-1}$ $T_a = -30.0°\ C$
$u_w = 3.0 \times 10^{-3}\ ms^{-1}$ $T_2 = -1.4°\ C$
$v_w = 3.0 \times 10^{-3}\ ms^{-1}$ $s_2 = 30.35\ psu$
$s_1 = 29.9\ psu$
$H = 1.0\ m$
$h = 30.0\ m$

75

CONDUCTIVE HEAT FLUX

SENSIBLE HEAT FLUX

OCEAN HEAT FLUX

76

ENTRAINMENT VELOCITY

TEMPERATURE DIFFERENCE (T1-T2)

SALINITY DIFFERENCE

77

SURFACE TEMPERATURE

ICE THICKNESS

MIXED LAYER DEPTH

Run 10:

$u_i = 0.1\ ms^{-1}$

$s_i = 9.0\ psu$

$v_i = 0.1\ ms^{-1}$

$u_w = 3.0 \times 10^{-3}\ ms^{-1}$

$v_w = 3.0 \times 10^{-3}\ ms^{-1}$

$s_1 = 29.9\ psu$

$H = 1.0\ m$

$h = 30.0\ m$

$u_{10} = 5.0\ ms^{-1}$

$v_{10} = 5.0\ ms^{-1}$

$T_e = -30.0°\ C$

$T_2 = -1.2°\ C$

$s_2 = 30.8\ psu$

INCOMING LONGWAVE RADIATION

OUTGOING LONGWAVE RADIATION

CONDUCTIVE HEAT FLUX

SENSIBLE HEAT FLUX

OCEAN HEAT FLUX

ENTRAINMENT VELOCITY

TEMPERATURE DIFFERENCE

SALINITY DIFFERENCE

81

SURFACE TEMPERATURE

ICE THICKNESS

MIXED LAYER DEPTH

82

Run 11:

INITIAL CONDITIONS :

u_i = 0.1 ms^{-1} u_{10} = 5.0 ms^{-1}

s_i = 9.0 psu v_{10} = 5.0 ms^{-1}

v_i = 0.1 ms^{-1} T_a = - 30.0° C

u_w = 3.0x10^{-3} ms^{-1} T_2 = - 1.4° C

v_w = 3.0x10^{-3} ms^{-1} s_2 = 30.8 psu

s_1 = 30.35 psu

H = 1.0 m

h = 30.0 m

INCOMING LONGWAVE RADIATION

OUTGOING LONGWAVE RADIATION

83

CONDUCTIVE HEAT FLUX

SENSIBLE HEAT FLUX

OCEAN HEAT FLUX

ENTRAINMENT VELOCITY

TEMPERATURE DIFFERENCE (T1-T2)

SALINITY DIFFERENCE (S1-S2)

85

SURFACE TEMPERATURE

ICE THICKNESS

MIXED LAYER DEPTH

86

LIST OF REFERENCES

Adamec, D., R. L. Elsberry, R. W. Garwood, and R. L. Haney, An embedded mixed layer-ocean circulation model, *Dyn. Atmos. Oceans*, 6, 69-96, 1981.

Andreas, E. L.., A theory for the scalar roughness and the scalar transfer coefficients over snow and sea ice, *Boundary-Layer Met.*, 38, 159-184, 1987.

Bauer, E., K. Hunkins, T. O. Manley and W. Tiemann, *Arctic Ice Dynamics Joint Experiment 1975-1976 Physical Oceanography Data Report, STD Data-Camp Caribou*, Volume 1. CU-8-80. Technical Report No. 8, Lamont-Doherty Geol. Obs. of Columbia Univ., Palisades, N.Y., 1980.

Chu, P. C., and R. W. Garwood, Comment on "A coupled dynamic-thermodynamic model of an ice-ocean system in the marginal ice zone", *J. Geophys. Res.*, 93, 5155-5156, 1988.

Claes, D. C., *Mixed Layer Dynamics in the Onset of Freezing*, Master's Thesis, Naval Postgraduate School, Monterey, California, December 1990.

Coachman, L. K., and K. Aagaard, Physical Oceanography of arctic and subarctic Seas, in *Marine Geology and Oceanography of the Arctic Seas*, edited by Y. Herman, pp.1-72, Springer-Verlag, N.Y., 1974.

Cox, G. F. N., and W. F. Weeks, Salinity variations in sea ice, *J. Galciol.*, 13, 109-20, 1974

Garwood, R. W., An oceanic mixed layer model capable of simulating cyclic states, *J. Phys. Oceanogr.*, 7, 455-468, 1977.

Gow, A. J., and W. B. Tucker, CRREL Monograph 91-1, *Physical and Dynamic Properties of Sea Ice in the Polar Oceans*, 46 pp., 1991.

Guest, P. S., and K. L. Davidson, The aerodynamic roughness of different types of sea ice, *J. Geophys. Res.*, 96, 4709-4721, 1991.

Hibler, W. D., and K. Bryan, A diagnostic ice-ocean model, *J. Phys. Oceanogr.*, 17, 987-1015, 1987.

Hibler,W. D. III, and W. B. Tucker, Some results from a linear viscous model of the Arctic ice cover, *J. Glaciol.*, 22, 293-304, 1979.

Kraus, E. B., and J. S. Turner, A one-dimensional model of the seasonal thermocline, *Tellus*, 19, 98-105, 1967.

Lemke, P., A coupled one-dimensional sea ice-ocean model, *J. Geophys. Res.*, 92, 13,164-13,172, 1987.

Maykut, G. A., Energy exchange over young sea ice in the central arctic, *J. Geophys. Res.*, 83, 3646-3658, 1978.

Maykut, G. A. , The ice environment, in *Sea Ice Biota*, edited by R. A. Horner, PP. 21-2, CRC Press, Boca Raton, Fl., 1985.

Maykut, G. A., The surface heat and mass balance, in *The Geophysics of Sea Ice*, NATO ASI Ser., vol. B 146, edited by N. Untersteiner, pp. 395-464, Plenum, New York, 1986.

Maykut, G. A., and P. E. Church, Radiation climate of Barrow, Alaska, 1962-66, *J. Appl. Met.*, 12, 620-628, 1973.

Maykut, G. A., and N. Untersteiner, Some results from a time dependent, Thermodynamic model of sea ice, *J. Geophys. Res.*, 76, 1550-1575, 1971

McPhee, M. G., The effect of the oceanic boundary layer on the mean drift of sea ice: Application of a simple model, *J. Phys. Oceanogr.*, 9, 388-400, 1979.

McPhee, M. G., Small scale processes, in *Polar Oceanography, Part A: Physical Science*, edited by W. O. Smith, Jr., pp. 287-334, Academic Press, San Diego, Ca., 1990.

McPhee, M. G., The upper ocean, in *The Geophysics of Sea Ice*, The NATO ASI Ser., vol. B 146, edited by N. Untersteiner, pp. 339-394, Plenum, New York, 1986.

Mellor, G. L.., and L. Kantha, An ice-ocean coupled model, *J. Geophys. Res.*, 94, 10,937-10,954, 1989.

Millero, F. J. and W. H. Leung, The thermodynamics of seawater at one atmosphere, *Amer. J. Sci.*, 276, 1035-1077, 1976.

88

Morison, J., and J. D. Smith, Seasonal variations in the upper Arctic Ocean as observed at T-3, *Geophys. Res. Lett.*, 8, 753-756, 1981.

Naval Polar Oceanography Center, *Ice Observation Handbook, 1984.*

Niiler, P. P., and E. B. Kraus, One dimensinal models of the upper ocean, in *Modeling and Prediction of the Upper Layers of the Ocean*, edited by E. B. Kraus, pp. 143-172, Pergamon Press, 1977.

Pollard, R. T., and R. C. Millard, Jr., Comparison between observed and simulated wind-generated inertial oscillations, *Deep-Sea Res.*, 17, 813-821, 1970.

Semtner, A. J., Jr., A numerical study of sea ice and ocean circulation in the arctic, *J. Phys. Oceanogr.*, 17, 1077-1099, 1987.

Stewart, R. H., *Methods of Satellite Oceanography*, University of California Press, pp. 360, 1985.

Stull, R. B., *An Introduction to Boundary Layer Meteorology*, Kluwer Academic Publishers, pp. 666, 1988.

Thorndike, A.S., A toy model linking atmospheric thermal radiation and sea ice growth, *J. Geophys. Res.*, 97, 9401-9410, 1992.

Thorndike, A. S., and R. Colony, Sea ice motion in response to geostrophic winds, *J. Geophys. Res.*, 87, 5845-5852, 1982

Untersteiner, N., On the mass and heat budget of arctic sea ice, *Arch. Meteorol. Geophys. Bioklimatol.*, Ser. A, 12, 151-182, 1961.

Untersteiner, N., Calculations of temperature regime and heat budget of sea ice in the central Arctic, *J. Geophys. Res.*, 69, 4755-4766, 1964.

Washington, W. M., A. J. Semtner, Jr., C. Parkinson, L. Morrison, On the development of a seasonal change sea-ice model, *J. Phys. Oceanogr.*, 6, 679-685, 1976.

Weeks, W. F., and S. F. Ackley, CRREL Monograph 82-1, *The Growth, Structure, and Properties of Sea Ice*, 130 pp. , 1982.

Zilitinkevich, S. S., D. V. Chalikov and Y. D. Resnyansky, Modelling the oceanic upper layer, *Oceanol. Acta.*, 2, 219-240, 1979.

INITIAL DISTRIBUTION LIST

No. Copies

1. Defense Technical Information Center   2
   Cameron Station
   Alexandria, VA 22304-6145

2. Library, Code 52   2
   Naval Postgraduate School
   Monterey, CA 93943-5000

3. Chairman (Code OC/Co)   1
   Department of Oceanography
   Naval Postgraduate School
   Monterey, CA 93943-5000

4. Chairman (Code MR/Hy)   1
   Department of Meteorology
   Naval Postgraduate School
   Monterey, CA 93943-5000

5. Prof. R. W. Garwood (Code OC/Gd)   2
   Department of Oceanography
   Naval Postgraduate School
   Monterey, CA 93943-5000

6. Prof. A. S. Thorndike   1
   Department of Physics
   University of Puget Sound
   Tacoma, WA 98416

7. LCDR B. R. Kitchen   1
   Cruiser-Destroyer Group One
   Unit 25064
   FPO AP 96601-4700

8. Director Naval Oceanography Division   1
   Naval Observatory
   34th and Massachusetts Avenue NW
   Washington, DC 20390

9. Commanding Officer   1
    Naval Oceanographic and Atmospheric Research Laboratory
    Stennis Space Center, MS 39529-5004

10. Commanding Officer   1
    Fleet Numerical Oceanography Center
    Monterey, CA 93943-5005

11. Commanding Officer   1
    Naval Polar Oceanography Center, Suitland
    Washington, DC 20373

12. Arlene Guest (Code OC/Gu)   1
    Department of Oceanography
    Naval Postgraduate School
    Monterey, CA 93943-5000